






Quantum Griffiths phase in disordered  $\text{Mn}_{1-x}\text{Fe}_x\text{Si}$ Ashish Kumar Mishra <sup>1,2</sup> S. Shanmukharao Samatham <sup>3,4,\*</sup> Mark T. F. Telling,<sup>5</sup> A. D. Hillier <sup>5</sup>  
Martin R. Lees <sup>6</sup> K. G. Suresh <sup>4</sup> and V. Ganesan<sup>2,7</sup><sup>1</sup>Department of Physics, Indian Institute of Science Education and Research Bhopal, Bhopal 462066, Madhya Pradesh, India<sup>2</sup>Low Temperature Laboratory, UGC-DAE Consortium for Scientific Research, Indore 452001, Madhya Pradesh, India<sup>3</sup>Department of Physics, Chaitanya Bharathi Institute of Technology, Gandipet, Hyderabad 500075, India<sup>4</sup>Magnetic Materials Laboratory, Department of Physics, Indian Institute of Technology Bombay, Mumbai 400076, Maharashtra, India<sup>5</sup>ISIS Pulsed Neutron and Muon Source, Science and Technology Facility Council, Rutherford Appleton Laboratory, Chilton, Didcot, Oxfordshire OX11 0QX, United Kingdom<sup>6</sup>Department of Physics, University of Warwick, Coventry CV4 7AL, United Kingdom<sup>7</sup>Medi-Caps University, AB Road, Pigdamber, Indore 453331, Madhya Pradesh, India

(Received 23 November 2022; revised 16 February 2023; accepted 17 February 2023; published 7 March 2023)

We show the presence of magnetic rare regions consistent with the quantum Griffiths phase in Fe-doped MnSi using detailed heat capacity, magnetization, and muon spin relaxation ( $\mu\text{SR}$ ) measurements down to millikelvin temperatures. The slow dynamics of these rare regions at low temperatures leads to the non-Fermi-liquid behavior in heat capacity and magnetization. The  $\mu\text{SR}$  and magnetization results further indicate that the dynamics freezes into a cluster-glass state below  $T_f \sim 1.25$  K. The results are in agreement with theoretical models proposed in the literature for metallic systems with Heisenberg symmetry that exhibit the quantum Griffiths phase in the presence of strong disorder.

DOI: [10.1103/PhysRevB.107.L100405](https://doi.org/10.1103/PhysRevB.107.L100405)

**Introduction.** Suppression of long-range magnetic order down to zero temperature,  $T = 0$  K, through some nonthermal control parameter ( $r$ ) such as pressure ( $p$ ), magnetic field ( $H$ ), or chemical doping ( $x$ ) results in a quantum critical point (QCP) [1,2]. However, ferromagnetic (FM) QCP in clean metals is interrupted by a first-order (FO) transition at a tricritical point (TCP) [3–7]. On the contrary, studies demonstrated that an intermediate disorder suppresses the TCP and restores the QCP [7–10]. Nevertheless, strong disorder can also lead to the formation of locally ordered rare regions irrespective of the disordered bulk system [11–13]. In addition, fluctuations of these rare regions near a quantum phase transition (QPT) completely modify the thermodynamic properties, resulting in a quantum Griffiths phase (QGP) [14]. The signatures of QGP include strong power-law singularities in temperature-dependent heat capacity  $C(T)/T$  and susceptibility  $\chi(T) \sim T^{\lambda-1}$  ( $0 < \lambda < 1$ ), indicating non-Fermi-liquid (nFL) behavior [1,11,13].

MnSi, known for its skyrmion lattice in the  $H$ - $T$  phase diagram [15,16], is a standard system for studying QCP due to its low ordering temperature,  $T_C \sim 30$  K [3,15,17]. Nonetheless, both pressure and doping studies established the presence of QPTs in  $p$ - $x$  and  $T$ - $x$  phase diagrams [3,4,9,10,18–29]. The pressure-induced QCP in MnSi at the critical pressure  $p_C \sim 14.6$  kbar, however, is still debated [30], as some results support the FO QPT [3,4], while others support the QCP or weak FO transition [29]. Contrary to that, doping studies in  $\text{Mn}_{1-x}\text{TM}_x\text{Si}$  ( $\text{TM} = \text{Cr}, \text{Fe}, \text{and Co}$ ), have shown the continuous suppression of  $T_C$  at QCP [18–28]. For example,

an earlier study in  $\text{Mn}_{1-x}\text{Fe}_x\text{Si}$  suggested a QCP at a critical concentration  $x_C \sim 0.192$  [27]. Hall and neutron scattering studies, on the other hand, discovered the suppression of long-range ordering (LRO) at  $x^* \sim 0.11$  hidden within the chiral fluctuations of short-range ordering (SRO) [20,24–26]. Interestingly, the studies [25,26] also suggested that this SRO vanishes at the second QCP  $x_C \sim 0.24$ . However, other studies [19,22,23] identified the  $x_C$  to be near 0.17 with vanishing of  $T_C$  and spontaneous magnetization along with a change in the sign of the Curie-Weiss temperature  $\theta_W$  from positive to negative. Nevertheless, with the LRO vanishing, Refs. [19,22,23] recognized  $x^*$  as a special point in the  $T$ - $x$  phase diagram. The region above  $x^*$  is also referred to as chiral spin liquid from its resemblance to a theoretically predicted blue fog phase above  $p_C$  in MnSi [25,31].

Even though there is general agreement in the literature that the LRO vanishes at  $x^* \sim 0.11$  [19,20,22–26], little attention has been paid to the region around the SRO vanishing at  $x_C$ . Although magnetization  $M(T)$  measurements [22,26] suggested the possibility of a glassy nature and Griffiths phase, its true nature remains unclear and requires further investigation. Moreover, studies attributed the presence of nFL behavior to QCP despite the fact that the nFL behavior is observed in an extended region of  $x$ . Essentially, the nature of QCP in  $\text{Mn}_{1-x}\text{Fe}_x\text{Si}$  in the presence of disorder remains unanswered and conclusions are mostly limited by the measurements of the properties down to 2 K.

In this work we present the evidence of an inhomogeneous nature of the magnetic system using microscopic muon spin relaxation ( $\mu\text{SR}$ ) measurements down to 75 mK. Together with magnetization and heat capacity results, we argue that the nFL behavior in  $\text{Mn}_{0.75}\text{Fe}_{0.25}\text{Si}$  is the result of a QGP

\*shanmukharao\_physics@cbit.ac.in

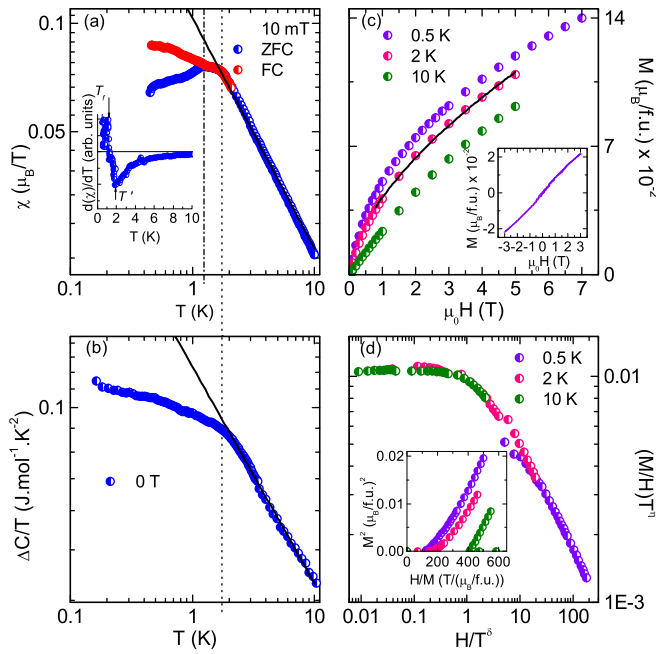


FIG. 1. (a)  $\chi(T)$  and (b)  $\Delta C(T)/T$  on a log-log scale. The vertical dash-dotted and dotted lines denote the transition to freezing temperature  $T_f$  and precursor state  $T'$  corresponding to the maxima and minima in  $d\chi(T)/dT$  [inset of (a)] respectively. (c)  $M$  vs  $H$  at three temperatures. Inset:  $M$ - $H$  hysteresis loop measured in low  $H$  at 500 mK. The black lines in (a), (b), and (c) are fit to a power-law divergence. (d) Scaling of  $(M/H)T^\eta$  vs  $H/T^\delta$ . Inset: Arrott plots at 0.5, 2.0, and 10 K.

different from a genuine QCP. The unique time window of the  $\mu$ SR technique,  $10^{-4} - 10^{-11}$  s, compared to ac susceptibility,  $10^1 - 10^{-3}$  s, and neutron scattering,  $10^{-9} - 10^{-12}$  s, allows us to probe the quasislow dynamics relevant to the present case.

**Results and Discussion.** Experimental details and related characterization specifications are given in the Supplemental Material (SM) [32] (see also Refs. [33,34] therein). Figure 1(a) shows the  $\chi(T) [\equiv M/H]$  of  $\text{Mn}_{0.75}\text{Fe}_{0.25}\text{Si}$  down to 500 mK, measured in 10 mT. The Curie-Weiss fit above 6 K provides the value of the effective magnetic moment  $\mu_{\text{eff}} = 1.17 \mu_B/\text{f.u.}$  and  $\theta_W = -3.57$  K (see Fig. S2 of SM). A negative  $\theta_W$  indicates that the average magnetic interactions within the alloy are antiferromagnetic (AFM). A clear bifurcation of zero-field-cooled (ZFC) and field-cooled (FC) curves below the peak temperature  $T_f \sim 1.25$  K suggest the freezing of the moments and may indicate glassy behavior of the system. However, the upward trend of the FC curve below  $T_f$  indicates the involvement of clusters, different from spin glass, where the FC curve remains flat [28,35,36]. Concomitantly, the absence of a sharp peak in  $\Delta C(T)/T$  down to 200 mK and only a slope change at  $T \sim 1.8$  K as shown in Fig. 1(b) support the absence of LRO in the system. Here,  $\Delta C = (C - C_{\text{lattice}})$  and the lattice contribution of the form  $C/T \sim T^2$  has been subtracted from  $C(T)$ . In addition, even at 500 mK, the  $M(H)$  curve measured up to 7 T lacks saturation [Fig. 1(c)]. The aforementioned facts, along with the S shape of the  $M(H)$  curve [inset of Fig. 1(c)] and the lack of spontaneous mag-

netization indicated by the Arrott plots [inset of Fig. 1(d)], which is typical of glassy behavior, demonstrate the spatially restricted nature of magnetism [36,37]. The nonlinearity in the  $M(H)$  curves up to 10 K indicates that spins have a finite correlation even in the paramagnetic (PM) region.

Additionally, a power-law fit to the curves  $\chi(T)$ ,  $\Delta C(T)/T$ , and  $M(H)$  of the form  $T^{-\eta}$  ( $\eta = 1 - \lambda$ ) provides the exponents  $\eta \sim 0.64$ , 0.54, and 0.6 and are shown in Figs. 1(a)–1(c), respectively. The observed power law, over a decade in  $T \sim 1.8 - 10$  K, is indicative of nFL behavior and allows us to recognize  $T^* \sim 10$  K as the temperature below which the dynamics of the clusters dominates. Furthermore, depending on the values of the exponent, one can assess the nature of the nFL behavior [38,39]. It is worth recalling that Moriya and Lonzarich [40,41] predicted  $\eta = 1.33$  for a three-dimensional (3D) FM QCP when compared to  $\eta = 1.5$  for a 3D AFM QCP [1,41]. On the other hand, for the nFL behavior originating from the disordered Kondo model, the exponent is calculated to be 0.75 [42]. Alternatively, for nFL systems described by a QGP, Neto and Jones proposed a power-law dependence  $\sim T^{\lambda-1}$  of  $\chi(T)$  and  $\Delta C(T)/T$  [43]. The values of  $\eta \sim 0.5 - 0.68$  in the present case are comparable to values  $\eta \in [0.67, 0.56]$  in disordered systems showing nFL behavior because of QGP [1].

Furthermore,  $M(H)$  isotherms of nFL systems are expected to follow a certain scaling given by the equation  $M/H = T^{-\eta} f(HT^{-\delta})$  [44,45]. Figure 1(d) shows the scaling plots of  $(M/H)T^\eta$  vs  $HT^{-\delta}$  with  $\eta = 0.64$  and  $\delta = 1.35$  which scale well and collapse onto a single universal curve. The exponent  $\delta$  is taken from our previous heat capacity scaling  $[C(T, H) - C(T, 0)]/T$  vs  $HT^{-\delta}$  [46]. The scaling exponents obtained for  $\text{Mn}_{0.75}\text{Fe}_{0.25}\text{Si}$  agree with the reported disordered nFL systems such as  $\text{CePd}_{0.85}\text{Rh}_{0.15}$  [39] and uranium-based alloys [44,45].

To further rule out the long-range ordering in  $\text{Mn}_{0.75}\text{Fe}_{0.25}\text{Si}$ , we have performed zero-field (ZF)- $\mu$ SR measurements down to 75 mK. Figures 2(a)–2(c) show the time dependence of the asymmetry  $A(t)$ . Mere a visual inspection of  $A(t)$  spectra suggests three different regions with decreasing temperature, i.e., (i)  $T \sim 40$  K, deep in the PM region with a Gaussian type of relaxation at earlier times and recovery of 1/3 tail at later times, (ii)  $T \leq 4$  K, a relatively fast damping at earlier times and slow damping of the tail at later times, and (iii)  $T \leq T_f \sim 1.25$  K, highly damped oscillations followed by a relatively slow damping of the tail at later times.

The ZF- $\mu$ SR spectra in the PM region are best described by the Kubo-Toyabe function times the stretched-exponential decay function

$$G_{\text{KT}}(t) = A_2 \left[ \frac{1}{3} + \frac{2}{3} (1 - \sigma_{\text{KT}}^2 t^2) e^{-\frac{\sigma_{\text{KT}}^2 t^2}{2}} \right] e^{(-\lambda_2 t)^\beta} + A_{\text{bg}}, \quad (1)$$

where  $\lambda_2$  is the relaxation rate associated with the dynamic electronic spin fluctuations,  $\beta$  is the stretched exponent related to the distribution of correlation times, and  $A_{\text{bg}}$  is a constant background arising from muons stopping on the silver sample holder. Its value, estimated at 40 K, was kept fixed for all the other spectra. The value of the nuclear depolarization rate,

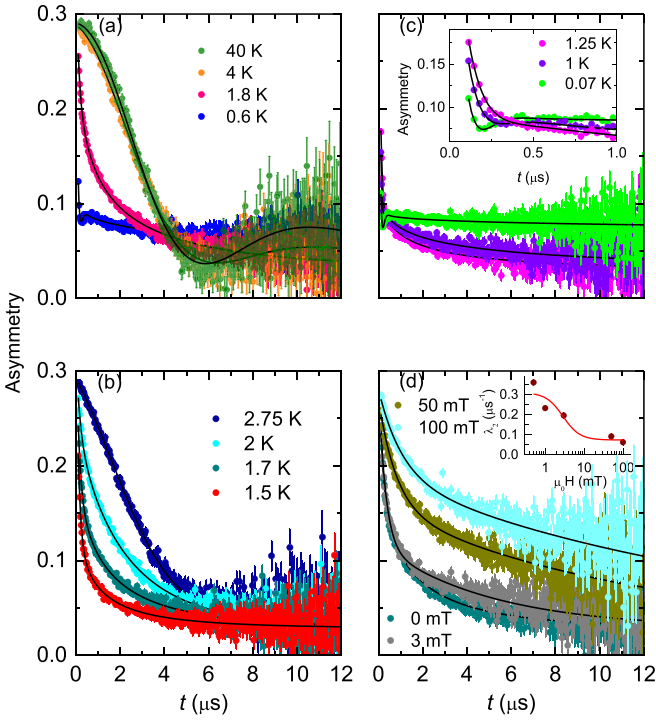


FIG. 2. (a)–(c) ZF- $\mu$ SR  $A(t)$  at a few representative temperatures from 40 to 75 mK. Inset of (c) shows  $A(t)$  at short times. (d) LF- $\mu$ SR  $A(t)$  at  $T = 1.7$  K for different  $H$ . The solid lines are the fits to the data using Eq. (3). Inset:  $\lambda_2(H)$  obtained using Eq. (3) and the red line is a fit.

$\sigma_{KT} \sim 0.28 \mu\text{s}^{-1}$ , at 40 K was found to be almost temperature independent.

On lowering the temperature below  $T_f \sim 1.25$  K, the ZF- $\mu$ SR spectra clearly show the presence of damped oscillations [Fig. 2(c)] and can be described by the function

$$A_{\text{osc}}(t) = A_1 \cos(2\pi ft + \varphi)e^{(-\lambda_1 t)}, \quad (2)$$

where  $\lambda_1$  is the muon depolarization rate arising from the distribution of the internal field,  $\varphi$  is the phase, and  $f$  is the muon precession frequency. However, the spectra in the whole temperature range are well described by a phenomenological function of the form [47]

$$A(t) = A_{\text{osc}}(t) + G_{KT}(t) \quad (3)$$

below 2 K,  $\sigma_{KT} = 0$ , and the  $G_{KT}(t)$  term simply becomes  $A_2 e^{(-\lambda_2 t)^\beta} + A_{\text{bg}}$ .

Various parameters such as  $f(T)$ ,  $\lambda_2(T)$ ,  $\lambda_1(T)$ , and  $\beta(T)$  obtained using Eq. (3) are shown in Figs. 3(a)–3(d), respectively.  $f(T)$ , which is proportional to the internal magnetic field, starts increasing only below 1.25 K. This corresponds to the  $T_f$  of  $\chi(T)$  and denotes the onset of magnetic correlations within the system. The slowing of the underlying magnetic entity dynamics is further evidenced by an increase in  $\lambda_2(T)$  on approaching  $T_f$  from the PM side, below which it begins to decrease, peaking at around 1.5 K. However, the lack of plateau in  $\lambda_2(T)$  down to lowest temperature in our case does not support the spin liquid state in  $\text{Mn}_{1-x}\text{Fe}_x\text{Si}$ , which otherwise is found true for spin liquid systems [48,49]. Besides, the sharp increase in  $\lambda_1(T)$  with a distinct slope

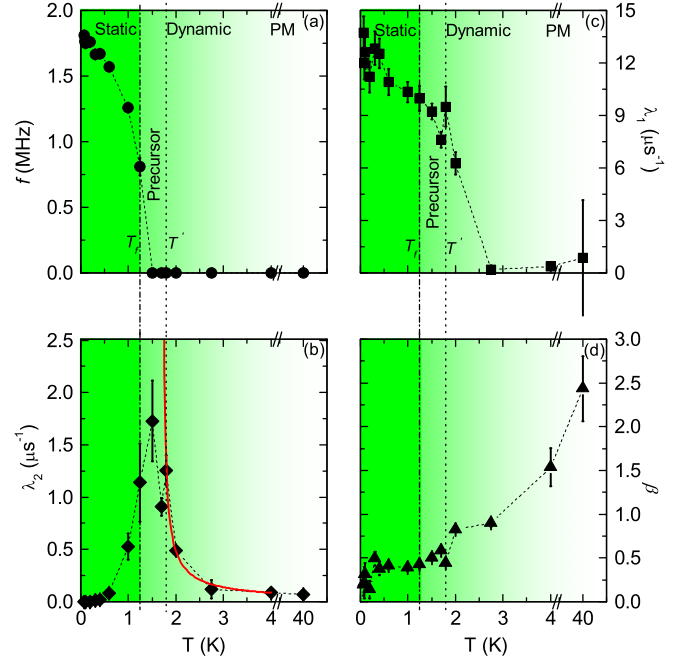


FIG. 3. (a)  $f(T)$ , (b)  $\lambda_2(T)$ , (c)  $\lambda_1(T)$ , and (d)  $\beta(T)$ , down to 75 mK obtained from fits of ZF- $\mu$ SR spectra using Eq. (3). The solid red line in (b) is a fit as described in the text. The transition to  $T_f$  and  $T'$  is denoted by vertical dash-dotted and dotted black lines in accordance with the  $\chi(T)$  and  $\Delta C(T)/T$ , respectively.

change near  $T_f \sim 1.25$  K indicates the presence of a broad distribution of the internal magnetic field due to the randomness present in the system. Nevertheless, the value of the  $\beta(T) \sim 1$  (representing a single relaxation time) at 2 K decreases with temperature to  $\beta(T) \sim 0.5$  at  $T_f$ , confirming that the distribution of relaxation time scales within the alloy [50]. Moreover, the average value of  $\beta \sim 1/3$  at low temperature indicates a concentrated spin glass different from the canonical spin-glass system [50,51]. Interestingly, small peaks in  $\lambda_1(T)$  and  $\lambda_2(T)$  could be seen at  $T' \sim 1.8$  K, which is also reflected as a dip in  $\beta(T)$  values. This matches well with the transition to a precursor state, as evident from the inflection in  $\chi(T)$  at 1.8 K. The LRO below  $T_f$  can be ruled out based on (i) the highly damped nature of oscillations in  $A(t)$ , (ii) the wide distribution of internal fields revealed from  $\lambda_1(T)$ , and (iii) the existence of magnetic entities with multiple relaxation rates revealed from  $\beta(T)$ . These results rather indicate the inhomogeneous nature or a glassy state of the magnetism below  $T_f$ , consistent with the  $\chi(T)$  and  $C(T)$  data. The results are similar to the glassy behavior found in the  $\text{Mn}_{1-x}\text{Co}_x\text{Si}$  for  $0.05 < x < 0.90$  [28].

To gain further insight into the glassy nature of the system, we fitted the divergence of  $\lambda_2(T)$  above  $T_f$  [Fig. 3(b)] to a critical scaling model  $\lambda_2(T) = \lambda_0 [T/T_g - 1]^{-\gamma}$ , which gives the glass transition temperature  $T_g = 1.70 \pm 0.15$  K and the critical exponent  $\gamma = 0.84 \pm 0.31$  [50]. The dynamic nature of the system near  $T_g$  is further confirmed using the Longitudinal-field (LF)- $\mu$ SR as shown in Fig. 2(d). The LF spectra measured at  $T = 1.7$  K in various  $H$  suggests that, in contrast to the PM region [10,52], application of a 100-mT field is insufficient to decouple the relaxation (also see Fig. S3

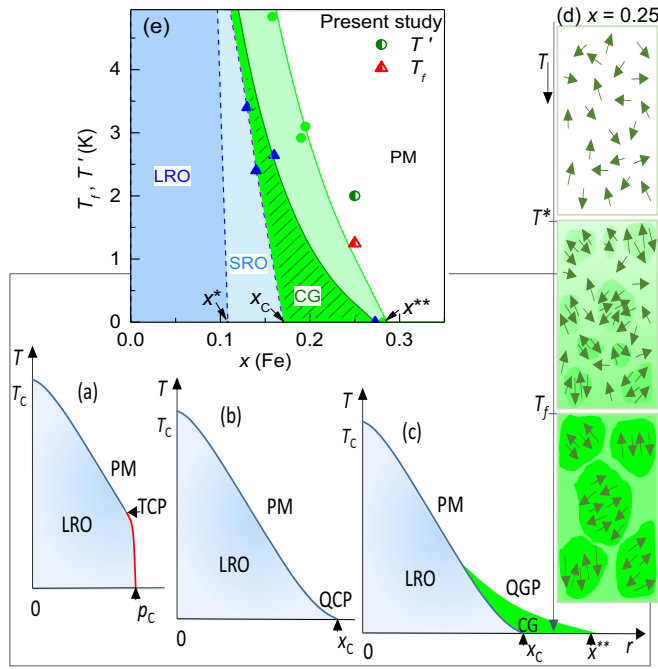


FIG. 4. Schematic illustration of  $T-x$  or  $p-x$  phase diagram with increasing disorder strength from (a) to (c) according to Ref. [8]. (a) Clean systems: resulting in FO QPT above TCP. (b) Intermediate disorder: resulting in a QCP. (c) Strong disorder: showing the effect of rare regions for Heisenberg symmetry [11–13]. Inset: (d) representing the survival of clusters and their freezing. (e)  $T-x$  phase diagram for  $\text{Mn}_{1-x}\text{Fe}_x\text{Si}$  showing the vanishing of  $T_f$  at  $x^{**}$ . Few data points are taken from Refs. [22,25,27].

[32]). Important information regarding spin-correlation time  $\tau_C$  and the fluctuating internal magnetic field  $H_{loc}$  at the muon site can be obtained from the Redfield equation  $\lambda_2 = \lambda_0 + 2(\gamma_\mu H_{loc})^2 \tau_C / [1 + (\gamma_\mu H_{LF} \tau_C)^2]$ . As shown in the inset of Fig. 2(d), the dynamic relaxation rate  $\lambda_2$  as a function of  $H$  fitted to the Redfield equation gives a value of  $\tau_C \sim 4.12 \times 10^{-7}$  s and  $H_{loc} \sim 0.63$  mT. The rather slow dynamics of around  $10^{-7}$  s in contrast to conventional spin-glass systems where the dynamics fall in the range  $10^{-9} - 10^{-11}$  s certainly indicate the involvement of spin clusters in this case [36,37,53]. The combined results of  $\chi(T)$ ,  $\Delta C(T)/T$ , and  $\mu\text{SR}$  obtained so far confirm three different regimes as a function of temperature: (i) PM above  $T^*$ , (ii) dynamic in the range  $T_f < T < T^*$ , and (iii) frozen state below  $T_f$ .

Qualitatively, the nFL behavior observed in  $\text{Mn}_{1-x}\text{Fe}_x\text{Si}$  above  $x_C \sim 0.17$  can be visualized from Fig. 4(d). The figure illustrates (i) the survival of the droplets of SRO with decreasing  $T$ , (ii) the slow dynamics of these growing rare regions leads to the observed QGP singularities below  $T^*$ , and (iii) the freezing of the dynamics in a random glassy fashion below  $T_f$ , resulting in a cluster-glass (CG) state. This is consistent with the theoretical arguments of Refs. [11–13]. For Heisenberg symmetry, the dimensionality of the rare regions  $d_{RR}$  lies exactly at the lower critical dimension of the phase transition  $d_C^-$ , forbidding independent ordering of the rare regions. The fluctuations of these rare regions lead to power-law divergence of the thermodynamic quantities, giving rise to QGP and nFL behavior at low temperatures. Moreover,

Ref. [13] further proposed that, at even lower temperatures, Ruderman-Kittel-Kasuya-Yosida (RKKY) interactions among rare regions completely freeze their dynamics, leading to the formation of a CG state and destroying the QGP singularities altogether [Fig. 4(c)]. Nevertheless, the presence of RKKY interaction in our case may support the localized nature of magnetism in  $\text{Mn}_{1-x}\text{Fe}_x\text{Si}$  as reported using Hall data [25].

Further, Fig. 4(e), shows the  $T-x$  phase diagram of  $\text{Mn}_{1-x}\text{Fe}_x\text{Si}$  in the region near  $x^*$  and  $x_C$ . The exponential fit of the data points suggests that both  $T_f$  and  $T'$  vanish completely only above  $x^{**} \sim 0.3$ . Since the average interaction changes from FM to AFM above  $x_C \sim 0.17$  [19,22,23,25], the present results then suggest a situation where the combined effect of disorder and frustration caused by random exchange interactions leads to clustering and their freezing in the tail region beyond  $x_C \sim 0.17$ . The slow dynamics of these rare clusters above  $x_C \sim 0.17$  gives rise to an extended region of QGP in the  $T-x$  phase diagram and contradicts the scenario of QCP, where the nFL behavior is observed close to  $x_C$  [1,2]. The results are similar to those for MnSi, where an extended region of nFL behavior is attributed to “partial order” below a characteristic temperature  $T_0$  that extrapolates to zero at a pressure  $p_0 \sim 21$  kbar [3]. The  $\mu\text{SR}$  report suggested the dynamic nature of this partial order in the range  $10^{-10} - 10^{-11}$  s [4]. Nevertheless, the lattice parameter  $a = 4.5403$  Å for  $\text{Mn}_{0.75}\text{Fe}_{0.25}\text{Si}$  in our case is comparable to the MnSi at  $p_0 \sim 21$  kbar [21]. The recent results [18,21] in  $\text{Mn}_{1-x}\text{Fe}_x\text{Si}$  and  $\text{Mn}_{1-x}\text{Co}_x\text{Si}$  attribute this similarity to MnSi to a cloud of critical fluctuations in an extended region of the  $T-x$  phase diagram. The surprising similarity between disordered and clean systems is, however, difficult to reconcile. Nevertheless, the study [54] suggested the role of minority phase droplets in the majority phase based on an entirely different mechanism of quenched disorder fluctuations near a FO transition. Nonetheless, the theoretical predictions of Refs. [7,8,11], appear to better describe the results in  $\text{Mn}_{1-x}\text{TM}_x\text{Si}$  ( $\text{TM} = \text{Cr}$  and Fe), where the disorder strength appears to have a progressive effect on the QPT in MnSi for different dopants. For example, FO QPT above TCP in MnSi with minimal disorder belongs to the case of a clean system [Fig. 4(a)]. On the other hand, our recent results in  $\text{Mn}_{1-x}\text{Cr}_x\text{Si}$  [9] with FM QCP and non-mean-field exponents belong to the case of intermediate disorder [Fig. 4(b)]. However, the present system  $\text{Mn}_{0.75}\text{Fe}_{0.25}\text{Si}$  with QGP is consistent with the case of strong disorder [Fig. 4(c)].

**Conclusions.** In summary, the combined results of magnetization, heat capacity, and  $\mu\text{SR}$  measurements suggest that the expected QCP in  $\text{Mn}_{1-x}\text{Fe}_x\text{Si}$  is avoided and the properties above  $x_C \sim 0.17$  are described by the formation of QGP at low temperatures due to the randomness generated by the strong disorder. The similar role of clusters giving rise to nFL behavior in systems such as  $\text{CeNi}_{1-x}\text{Cu}_x$  [55],  $\text{CePd}_{1-x}\text{Rh}_x$  [56], and  $\text{Ni}_{1-x}\text{V}_x$  [57] indicates a generic route to prevent FM QCP in the presence of strong disorder.

**Acknowledgments.** The authors thank DST-India for supporting the LTHM facility, Physical Property Measurement System (Quantum Design, USA). P. Saravanana, Cryogenics is thanked for his timely support. A.K.M. acknowledges SERB, India for NPDF [Grant

No. PDF/2021/002916]. A.K.M. acknowledges CSIR, India for SRF [Grant No. 09/926(0011)2K18]. S.S.S. thanks financial support from IIT Bombay through Institute

Post-Doctoral Fellow scheme. A.K.M., S.S.S., and V.G. acknowledge support from Newton-India (Experiment No. RB1620085) to perform  $\mu$ SR measurements at EMU.

- [1] G. R. Stewart, *Rev. Mod. Phys.* **73**, 797 (2001).
- [2] H. V. Löhneysen, A. Rosch, M. Vojta, and P. Wölfle, *Rev. Mod. Phys.* **79**, 1015 (2007).
- [3] C. Pfleiderer, P. Böni, T. Keller, U. K. Rößler, and A. Rosch, *Science* **316**, 1871 (2007).
- [4] Y. J. Uemura, T. Goko, I. M. Gat-Malureanu, J. P. Carlo, P. L. Russo, A. T. Savici, A. Aczel, G. J. MacDougall, J. A. Rodriguez, G. M. Luke, S. R. Dunsiger, A. McCollam, J. Arai, C. Pfleiderer, P. Böni, K. Yoshimura, E. Baggio-Saitovitch, M. B. Fontes, J. Larrea, Y. V. Sushko, and J. Sereni, *Nat. Phys.* **3**, 29 (2007).
- [5] M. Uhlarz, C. Pfleiderer, and S. M. Hayden, *Phys. Rev. Lett.* **93**, 256404 (2004).
- [6] C. Pfleiderer and A. D. Huxley, *Phys. Rev. Lett.* **89**, 147005 (2002).
- [7] D. Belitz, T. R. Kirkpatrick, and T. Vojta, *Phys. Rev. Lett.* **82**, 4707 (1999).
- [8] Y. Sang, D. Belitz, and T. R. Kirkpatrick, *Phys. Rev. Lett.* **113**, 207201 (2014).
- [9] A. K. Mishra, S. Shanmukharao Samatham, M. R. Lees, and V. Ganesan, *Phys. Rev. B* **101**, 144436 (2020).
- [10] T. Goko, C. J. Arguello, A. Hamann, T. Wolf, M. Lee, D. Reznik, A. Maisuradze, R. Khasanov, E. Morenzoni, and Y. J. Uemura, *npj Quant. Mater.* **2**, 44 (2017).
- [11] T. Vojta and J. Schmalian, *Phys. Rev. B* **72**, 045438 (2005).
- [12] T. Vojta, *J. Low Temp. Phys.* **161**, 299 (2010).
- [13] V. Dobrosavljevic and E. Miranda, *Phys. Rev. Lett.* **94**, 187203 (2005).
- [14] R. Griffiths, *Phys. Rev. Lett.* **23**, 17 (1969).
- [15] S. Mühlbauer, B. Binz, F. Jonietz, C. Pfleiderer, A. Rosch, A. Neubauer, R. Georgii, and P. Böni, *Science* **323**, 915 (2009).
- [16] S. S. Samatham and V. Ganesan, *Phys. Status Solidi RRL* **7**, 184 (2013).
- [17] Y. Ishikawa, T. Tajima, D. Bloch, and M. Roth, *Solid State Commun.* **19**, 525 (1976).
- [18] A. E. Petrova, S. Y. Gavrilkin, A. Y. Tsvetkov, Dirk Menzel, Julius Greife, S. Khasanov, and S. M. Stishov, *Phys. Rev. B* **106**, 014406 (2022).
- [19] C. Pappas, A. O. Leonov, L. J. Bannenberg, P. Fouquet, T. Wolf, and F. Weber, *Phys. Rev. Res.* **3**, 013019 (2021).
- [20] J. Kindervater, T. Adams, A. Bauer, F. X. Haslbeck, A. Chacon, S. Mühlbauer, F. Jonietz, A. Neubauer, U. Gasser, G. Nagy, N. Martin, W. Häußler, R. Georgii, M. Garst, and C. Pfleiderer, *Phys. Rev. B* **101**, 104406 (2020).
- [21] A. E. Petrova, S. Y. Gavrilkin, D. Menzel, and S. M. Stishov, *Phys. Rev. B* **100**, 094403 (2019).
- [22] L. J. Bannenberg, F. Weber, A. J. E. Lefering, T. Wolf, and C. Pappas, *Phys. Rev. B* **98**, 184430 (2018).
- [23] L. J. Bannenberg, R. M. Dalgliesh, T. Wolf, F. Weber, and C. Pappas, *Phys. Rev. B* **98**, 184431 (2018).
- [24] S. V. Demishev, A. N. Samarin, J. Huang, V. V. Glushkov, I. I. Lobanova, N. E. Sluchanko, N. M. Chubova, V. A. Dyadkin, S. V. Grigoriev, M. Y. Kagan, J. Vanacken, and V. V. Moshchalkov, *JETP Lett.* **104**, 116 (2016).
- [25] V. V. Glushkov, I. I. Lobanova, V. Y. Ivanov, V. V. Voronov, V. A. Dyadkin, N. M. Chubova, S. V. Grigoriev, and S. V. Demishev, *Phys. Rev. Lett.* **115**, 256601 (2015).
- [26] S. V. Demishev, I. I. Lobanova, V. V. Glushkov, T. V. Ischenko, N. E. Sluchanko, V. A. Dyadkin, N. M. Potapova, and S. V. Grigoriev, *JETP Lett.* **98**, 829 (2014).
- [27] A. Bauer, A. Neubauer, C. Franz, W. Münzer, M. Garst, and C. Pfleiderer, *Phys. Rev. B* **82**, 064404 (2010).
- [28] J. Teyssier, E. Giannini, V. Guritanu, R. Viennois, D. van der Marel, A. Amato, and S. N. Gvasaliya, *Phys. Rev. B* **82**, 064417 (2010).
- [29] A. E. Petrova and S. M. Stishov, *Phys. Rev. B* **86**, 174407 (2012).
- [30] C. Pappas, L. J. Bannenberg, E. Lelièvre-Berna, F. Qian, C. D. Dewhurst, R. M. Dalgliesh, D. L. Schlagel, T. A. Lograsso, and P. Falus, *Phys. Rev. Lett.* **119**, 047203 (2017).
- [31] S. Tewari, D. Belitz, and T. R. Kirkpatrick, *Phys. Rev. Lett.* **96**, 047207 (2006).
- [32] See Supplemental Material at <http://link.aps.org/supplemental/10.1103/PhysRevB.107.L100405> for the details of sample preparation, characterization, and description of muon spin relaxation technique.
- [33] J. Rodriguez-Carvajal, *Phys. B (Amsterdam, Neth.)* **192**, 55 (1993).
- [34] C. Magen, P. A. Algarabel, L. Morellon, J. P. Araújo, C. Ritter, M. R. Ibarra, A. M. Pereira, and J. B. Sousa, *Phys. Rev. Lett.* **96**, 167201 (2006).
- [35] D. A. Pejakovic, J. L. Manson, J. S. Miller, and A. J. Epstein, *Phys. Rev. Lett.* **85**, 1994 (2000).
- [36] J. A. Mydosh, *Spin Glasses: An Experimental Introduction* (Taylor & Francis, London, 1993).
- [37] K. Binder and A. P. Young, *Rev. Mod. Phys.* **58**, 801 (1986).
- [38] J. G. Sereni, T. Westerkamp, R. Küchler, N. Caroca-Canales, P. Gegenwart, and C. Geibel, *Phys. Rev. B* **75**, 024432 (2007).
- [39] D. T. Adroja, A. D. Hillier, J. G. Park, W. Kockelmann, K. A. McEwen, B. D. Rainford, K. H. Jang, C. Geibel, and T. Takabatake, *Phys. Rev. B* **78**, 014412 (2008).
- [40] T. Moriya, *Spin Fluctuations in Itinerant Electron Magnetism* (Springer-Berlin, New York, 1985).
- [41] G. G. Lonzarich, *The Electron* (Cambridge University Press, Cambridge, UK, 1997).
- [42] D. R. Grempel and M. J. Rozenberg, *Phys. Rev. B* **60**, 4702 (1999).
- [43] A. H. C. Neto and B. A. Jones, *Phys. Rev. Lett.* **81**, 3531 (1998).
- [44] B. Andraka and A. Tsvetkov, *Phys. Rev. Lett.* **67**, 2886 (1991).
- [45] A. M. Tsvetkov and M. Reizer, *Phys. Rev. B* **48**, 9887 (1993).
- [46] S. S. Samatham, S. Yadam, D. Singh, and V. Ganesan, *J. Magn. Magn. Mater.* **418**, 289 (2016).

- [47] A. Bhattacharyya, D. D. Khalyavin, D. T. Adroja, A. M. Strydom, A. D. Hillier, P. Manuel, T. Takabatake, J. W. Taylor, and C. Ritter, *Phys. Rev. B* **90**, 174412 (2014).
- [48] L. Clark, J. C. Orain, F. Bert, M. A. De Vries, F. H. Aidoudi, R. E. Morris, P. Lightfoot, J. S. Lord, M. T. F. Telling, P. Bonville, J. P. Attfield, P. Mendels, and A. Harrison, *Phys. Rev. Lett.* **110**, 207208 (2013).
- [49] B. Fåk, E. Kermarrec, L. Messio, B. Bernu, C. Lhuillier, F. Bert, P. Mendels, B. Koteswararao, F. Bouquet, J. Ollivier, A. D. Hillier, A. Amato, R. H. Colman, and A. S. Wills, *Phys. Rev. Lett.* **109**, 037208 (2012).
- [50] M. T. F. Telling, K. S. Knight, F. L. Pratt, A. J. Church, P. P. Deen, K. J. Ellis, I. Watanabe, and R. Cywinski, *Phys. Rev. B* **85**, 184416 (2012).
- [51] I. A. Campbell, A. Amato, F. N. Gygax, D. Herlach, A. Schenck, R. Cywinski, and S. H. Kilcoyne, *Phys. Rev. Lett.* **72**, 1291 (1994).
- [52] R. S. Hayano, Y. J. Uemura, J. Imazato, N. Nishida, T. Yamazaki, H. Yasuoka, and Y. Ishikawa, *Phys. Rev. Lett.* **41**, 1743 (1978).
- [53] Y. J. Uemura, T. Yamazaki, R. S. Hayano, and R. Nakai, *Phys. Rev. Lett.* **45**, 583 (1980).
- [54] T. R. Kirkpatrick and D. Belitz, *Phys. Rev. B* **93**, 144203 (2016).
- [55] N. Marcano, J. C. Gomez Sal, J. I. Espeso, J. M. De Teresa, P. A. Algarabel, C. Paulsen, and J. R. Iglesias, *Phys. Rev. Lett.* **98**, 166406 (2007).
- [56] T. Westerkamp, M. Deppe, R. Kuchler, M. Brando, C. Geibel, P. Gegenwart, A. P. Pikul, and F. Steglich, *Phys. Rev. Lett.* **102**, 206404 (2009).
- [57] R. Wang, A. Gebretsadik, S. Ubaid-Kassis, A. Schroeder, T. Vojta, P. J. Baker, F. L. Pratt, S. J. Blundell, T. Lancaster, I. Franke, J. S. Möller, and K. Page, *Phys. Rev. Lett.* **118**, 267202 (2017).